Sensitive and selective detection of uranyl ions based on aggregate-breaking mechanism

Xuan-Qui Pham, Naresh Kumar, Minh-Huong Ha-Thi, Isabelle Leray

Sensitive and selective detection of uranyl ions based on aggregate-breaking mechanism

Xuan-Qui Pham[a] , Naresh Kumar[a], Minh-Huong Ha-Thi[a],[b], Isabelle Leray[a*]

a PPSM, ENS Paris Saclay, CNRS, Université Paris Saclay

61 avenue du Président Wilson, 94235 Cachan Cedex, France

E-mail: isabelle.leray@ens-paris-saclay.fr

b Institut des Sciences Moléculaire d'Orsay (ISMO), CNRS, Univ. Paris-Sud, Université Paris Saclay, F-91405 Orsay, France

Abstract: A highly selective fluorescent sensor based on salicylaldehyde azine derivative for the detection of uranyl cation was developed. The aggregation induced emission characteristics of compounds S1 and S2 were investigated and a strong emission of these derivatives was observed upon aggregation in organoaqueous solvent. The emission of these aggregated forms was found to be effectively quenched by uranyl cation. In water/acetonitrile (60/40; v/v), the aggregates of S2 gave the most obvious quenching effect. The effect of uranyl was shown to be destructive rather than constructive to the aggregation of the salicylaldehyde azine derivatives. An aggregate-breaking process was proposed to explain the destruction of the aggregates by the complexation with uranyl cation. S2 can be used as an efficient fluorescent sensor for uranyl cation in aqueous solvent. The sensor showed good selectivity towards uranyl and with a low detection limit up to ppb scale.

1. Introduction

Uranium, a radioactive element has been extensively used in the nuclear industry. The fissile isotope ^{235}U plays a principal role in the development of nuclear power plants and nuclear weapons, with ^{235}U being the first material pursued in the development of the atomic bombs deployed during World War II.

Atomic weapons and fissile materials are ongoing concerns for human safety.[1] ^{238}U has been used in advanced nuclear reactors as a source material for creating plutonium-239, which can in turn be used as a nuclear power source. Increasing human activities with uranium have consequently led to widespread pollution and environmental impact. The uranyl ion (UO_2^{2+}) is a naturally occurring oxycation found in minerals and has been reported to cause birth defects and immune system damage.[2] The maximum allowable concentration of uranyl in drinking water has been defined as 20 ppb by the World Health Organization. Keeping in view the importance of the uranyl ion, sensitive and selective protocols for the detection of these ions are in great demand.[3] Analytical techniques such as potentiometry, X-ray fluorescence, ICP-MS, and ion-chromatography have been used for uranyl detection.[4-8] Alternatively, absorbance or emission-based optical sensors can also provide unique advantages. For example, several inorganic fluorescent sensors have been reported such as phosphate or pyrophosphate salts.[9-11] One of the disadvantages is that they are often interfered by other cations at low temperature due to crystallization.

Several organic fluorescent sensors based on 2,6-pyridinedicarboxylic acid,[12] quinoxalinol salen ligands,[13] cyclic peptide,[14] clopidogrel,[15] polymer containing amidoxime,[16] and salicylaldehyde azine[17] were reported to detect uranyl cations up to ppm or ppb scale. However, the common problems of organic fluorescent sensors are a lack of selectivity from other lanthanides and the limitation of working in aqueous solution.[18-24]

Our research group has been working on the design and the synthesis of fluorescent sensors for ions of biological or environmental significance.[25, 26][27-29]. In continuation of this work, we herein report two analogous compounds (S1 and S2). Their photophysical and complexing properties for uranyl ions have been investigated. The presence of nitro groups on aromatic rings in the S2 compounds might have an effect on the electron density at hydroxy and Schiff-base centers, and on the aggregation behavior in organoaqueous media. S2 was shown to be a highly selective and sensitive sensor for UO_2^{2+} detection in aqueous solvent.

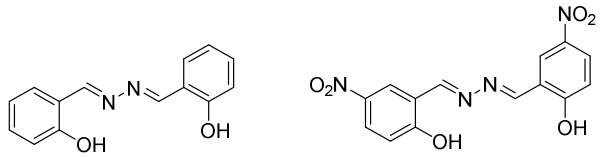

Figure 1. Structure of studied salicylaldehyde azine derivatives.

2. Experimental section

2.1 Synthesis

General procedure

All reagents were purchased from Aldrich and were used without further purification. ^{1}H and ^{13}C spectra were recorded on a JEOL-FT NMR 400 MHz spectrophotometer using CD_3OD/DMSO-d_6 as solvent and tetramethylsilane as internal standard. Data are reported as follows: chemical shift in ppm (δ), multiplicity (s = singlet, d = doublet, t = triplet, m = multiplet), coupling constants J (Hz).

N,N/-bis(salicylidene)hydrazine) **S1**

Compound S1 was synthesized via a previously reported procedure.[30] Firstly, salicylaldehyde (500 mg, 4.098 mmol) was dissolved completely in 40 mL ethanol. Hydrazine hydrate (102 mg, 2.041 mmol) solution in ethanol (20 mL) was then added over at least 20 min. After that, the resulting reaction mixture was refluxed for 4 hours. After cooling to room temperature, a yellow solid was formed, filtered and washed with cold ethanol to give pure product in 90% yield. ^{1}H NMR (CD_3OD, 400 MHz): δ = 11.40 (s, 2 H), 8.71 (s, 2 H), 7.38 (m, 4 H), 7.05 (d, 2 H), 6.97 (t, 2 H) ppm.

N,N/-bis(5-nitro-salicylidene)hydrazine **S2**

Compound S2 was synthesized using a similar procedure.[31] 2-hydroxy-5-nitrobenzaldehyde (500 mg, 2.99 mmol) was dissolved in 30 mL ethanol, following by the addition of hydrazine hydrate (74.8 mg, 1.50 mmol) solution in 15 mL ethanol. After that, the resulting reaction mixture was refluxed for 4 hours. After cooling to room temperature, a yellow solid was formed, filtered and washed with cold ethanol to give pure product in 91% yield. ^{1}H NMR (DMSO, 400 MHz): δ = 9.08 (s, 2 H), 8.70 (d, 2 H), 8.27 (dd, 2 H), 7.16 (dd, 2 H) ppm.

2.2. Spectroscopic measurement

2.2.1 Solvents and Salts. Acetonitrile from Aldrich (spectroscopic grade) was employed as solvent for absorption and fluorescence measurements. Cations from Aldrich or Alfa Aesar, were of the highest quality available and vacuum dried over P_2O_5 prior to use.

2.2.2 UV-visible absorption spectroscopy

For all absorption spectroscopy measurements, Hellma quartz cells with an inner path length of 10 mm were used. Double beam Varian Cary-4000 and Cary-5000 spectrophotometers were used to record the UV-visible absorption spectra.

2.2.3 Steady state fluorescence spectroscopy

For all fluorescence spectroscopy measurements, Hellma quartz cells with an inner path length of 10 mm were used. Corrected emission spectra were obtained on a Jobin–Yvon SPEX Fluoromax-4 spectrofluorometer.

2.3. Photophysical and complexation studies

For studies in dilute solution, compounds S1 and S2 were dissolved in acetonitrile with [S1] = 5 µM and [S2] = 7 µM. For AIE studies, water was added as a second, poor-soluble solvent was added and increased gradually by each 10%, from 0% to 100%. The samples were put in the dark under a luminescence source to quickly evaluate their emission intensity. The fluorescence quantum yield of each sample was calculated using quinine sulfate in sulfuric acid 0.5 N as a reference.[32] In all experiments, the ligands were excited at 365 nm and fluorescence spectra was recorded at 550 nm. All spectroscopic data of the complexation were recorded after one hour in the dark to make sure that the aggregation behaviors were completed.

For selectivity studies, the detection limit towards uranyl was calculated based on the quenching response of **S2** at a small concentration range of uranyl (0-3 µM). The following equation was used to calculate the detection limit: $c_{limit} = 3s / k$, where s represents the standard deviation of S2 solution, c_{limit} is the limit of detection and k is the slope of the working curve.

The concentration of S2 was 7 µM. All samples were excited at 365 nm and fluorescence intensities were recorded at 550 nm. The concentration of uranyl and competing cation were 20 µM and the reaction time was also one hour.

2.4 Dynamic Light Scattering

The sizes of aggregates were obtained by DLS by means of an analyzer Zetasizer Nano ZS ZEN 3600. There is a 4 mW He–Ne laser, operating at 633 nm, and a photomultiplier detector capable of collecting backscattered light at 175°. The temperature during analysis was 25 °C.

Measurements of intensity were performed in a multi-acquisition mode with automatically adjusted correlograms. Average sizes of aggregates and distribution widths were calculated by fitting the correlogram with a cumulants algorithm.

2.5 Scanning Electron Microscopy

Electron images were obtained by The Hitachi S-3400N equipped with Secondary and Backscatter Electron Detectors. There is a Deben Peltier Coolstage to control moisture loss in low vacuum mode.

3. Results and discussion

Synthesis

Compound S1 and S2 were synthesized according to previously reported procedures [30, 31] and can be obtained in high yields by the condensation of salicylaldehyde and 5-nitro salicylaldehyde, respectively, with hydrazine in ethanol.

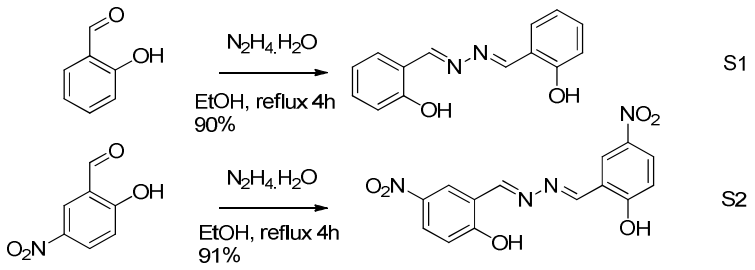

Scheme 1. Synthesis of sensors S1 and S2.

Aggregation-induced emission properties

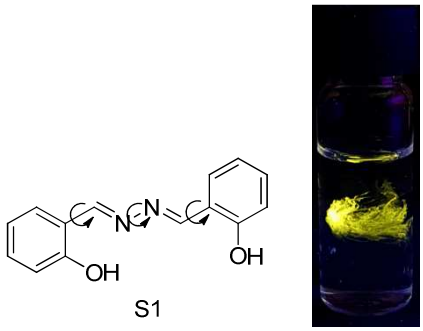

Scheme 2. Structure of S1 with free C-C; N-N rotation (left) and its emissive aggregate in water (right).

An emissive aggregate / nanosuspension was formed immediately after the injection of S1 solution in acetonitrile to water (Scheme 2), which might suggest that S1 has aggregation induced emission (AIE) characteristics in water/acetonitrile solution. In fact, in water/acetonitrile with a percentage of water less than 80%, S1 (5 µM) was well dispersed in the solution. Consequently, the molecules were conformationally flexible along with a free intramolecular rotation of carbon-carbon that leads to non-radiative decay processes. In this condition, fluorescence was quenched so that almost no emission was observed. When the percentage of water reached 80% or more, S1 molecules began to aggregate and free intramolecular rotation was restricted. Consequently, the non-radiative decay processes were hampered and the fluorescence intensity showed a corresponding increase (Figure and figure 3). Similar behavior was also reported for this molecule in the water/ethanol mixture.[30]

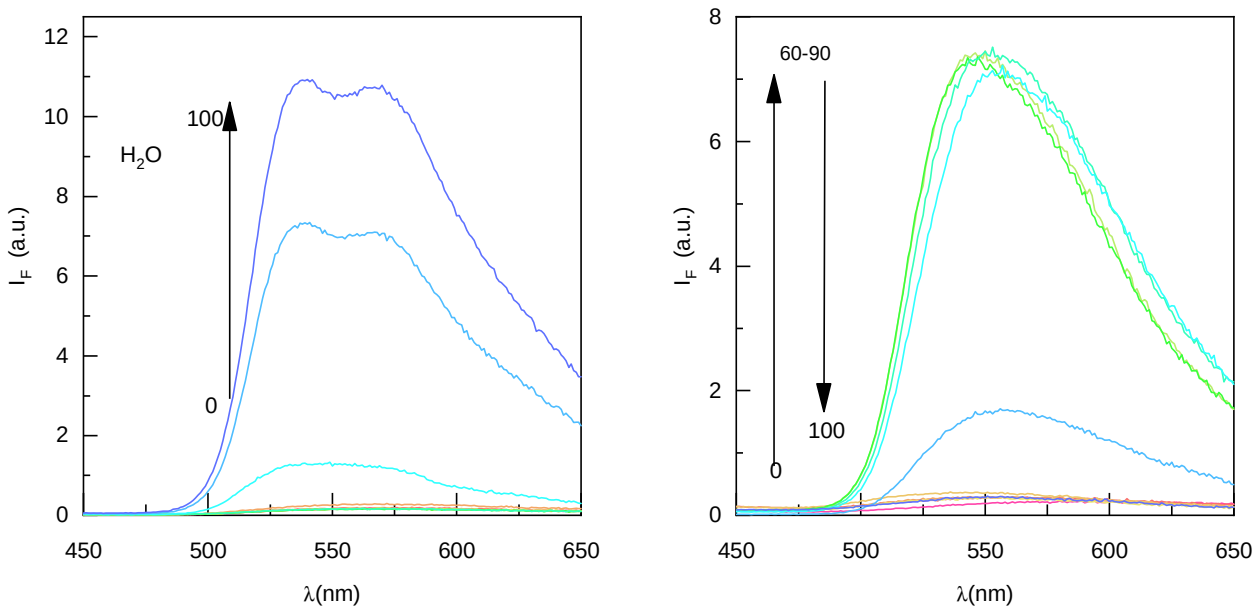

Figure 2 Emission spectra of S1 (5μM) (left) and S2 (7 μM) (right) with different fraction H_2O/CH_3CN (v:v), λ_{exc} = 365 nm

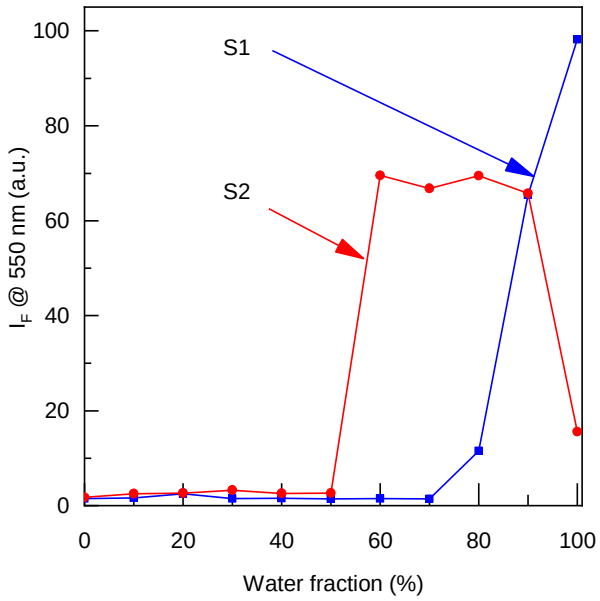

Figure 3. Changes in fluorescence intensity at 550 nm of S1 and S2 as water fraction in acetonitrile (v/v) increased. λ_{exc} = 365 nm. [S1] = 5 µM, [S2] = 7 µM.

Compound S2 also shows aggregation induced emission. In a well-dissolved solution, the molecule displays very poor fluorescence. Up to 60% water fraction or more, the molecules started to aggregate and the fluorescence intensity was quickly enhanced. While S1 molecules aggregated considerably at 90% water fraction, fluorescence of S2 was already strong when water fraction reached to 60% (Figure and figure 4). This can be rationalized by the lower solubility of S2 due to the presence of two nitro groups.

The viscosity of a solution, which can be affected by temperature, can modify the fluorescence of a compound. To gain more insight into this effect, temperature dependence of the fluorescence properties of compound S2 was studied. For this purpose, propylene glycol was used to increase viscosity withdecreasing of temperature without crystallization. At low temperature, as the solvent becomes more viscous, the rotation of intramolecular bonds would become restricted. S2 and a reference fluorophore, BODIPY (Fig. S4), were dissolved in propylene glycol to monitor the fluorescence change with decreasing temperature. Fluorescence spectra of S2 during temperature variations and its comparison with temperature dependent fluorescence changes of BODIPY are shown in Figures 4 and 5, respectively.

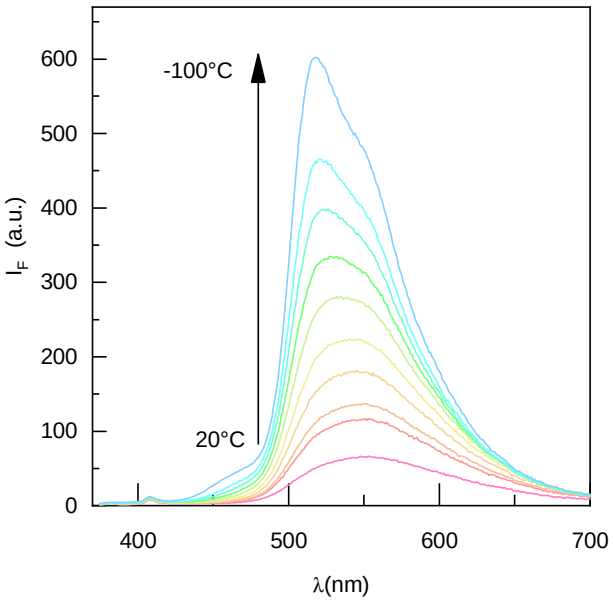

Figure 4. Fluorescence spectra of S2 (in propylene glycol) when temperature decreases gradually to -100°C. [S2] = 10 µM. λ_{exc} = 365 nm.

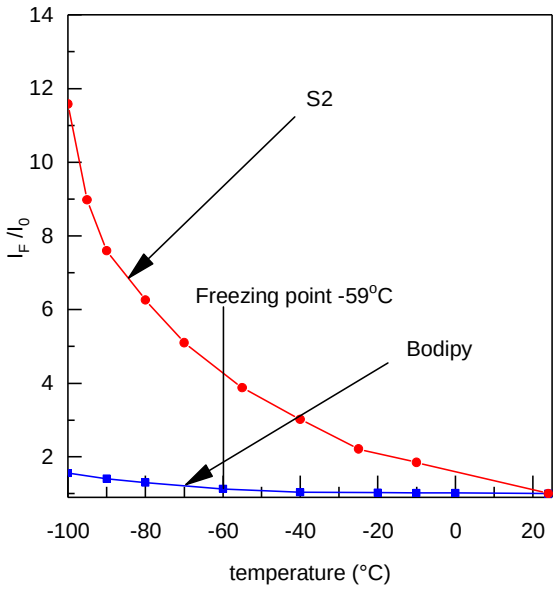

Figure 5. Comparison of fluorescence spectra changes of reference BODIPY (Blue) and S2 (red) in propylene glycol at different temperatures. [S2] = 10 µM, λ_{exc} = 365 nm, λ_{obs} = 520 nm. [BODIPY] = 10 µM, λ_{exc} = 510 nm, λ_{obs} = 530 nm.

Fluorescence spectra of BODIPY and S2 showed a shift to shorter wavelength as temperature decreased. Such blue shifts of fluorophores at lower temperature were reported previously.[33-35] Moreover, fluorescence enhancement by decreasing temperature was observed in both cases. From room temperature to -100°C, fluorescence intensity of BODIPY at 530 nm was increased about 2 times while fluorescence intensity of S2 at 520 nm was increased more than 10 times. The restriction of intramolecular rotation in S2 might explain this difference. The decrease of temperature could reduce the molecular collisions and the non-radiative pathways. Once the temperature became lower than the freezing point of propylene glycol (-59°C), rotational motion was mostly prevented, particularly for the case of AIE dyes like S2. The difference in fluorescence behavior between two molecules gives a clear confirmation of the effect of molecular rotation on the fluorescence characteristics of S2, where the fluorescence was dramatically enhanced in a rigid medium.

Complexing properties of sensors with the uranyl cation

The sensors were expected to form a complex with uranyl cations owing to the presence of nitrogen and oxygen atoms in the molecular scaffold. The complexation can disturb the aggregation behavior and have a significant influence on the fluorescence of the AIE dyes. Fluorescence changes of S1 (5 μM) and S2 (7 μM) in different water/acetonitrile mixtures were evaluated by adding an excess amount of uranyl cation (50 μM). All spectroscopic data were recorded after one hour in order to complete the complexation.

The addition of uranyl cation to well dispersed solutions of S1 and S2 did not enhance the fluorescence. However, fluorescence of S1 and S2 aggregates was partially quenched upon addition of uranyl after one hour. The fluorescence response of S1 and S2 aggregates at different water fractions with uranyl cation is shown in

Figure 3 and Figure 4, respectively. A smaller fraction of water granted no significant fluorescence changes as aggregates were non-emissive in dilute solution.

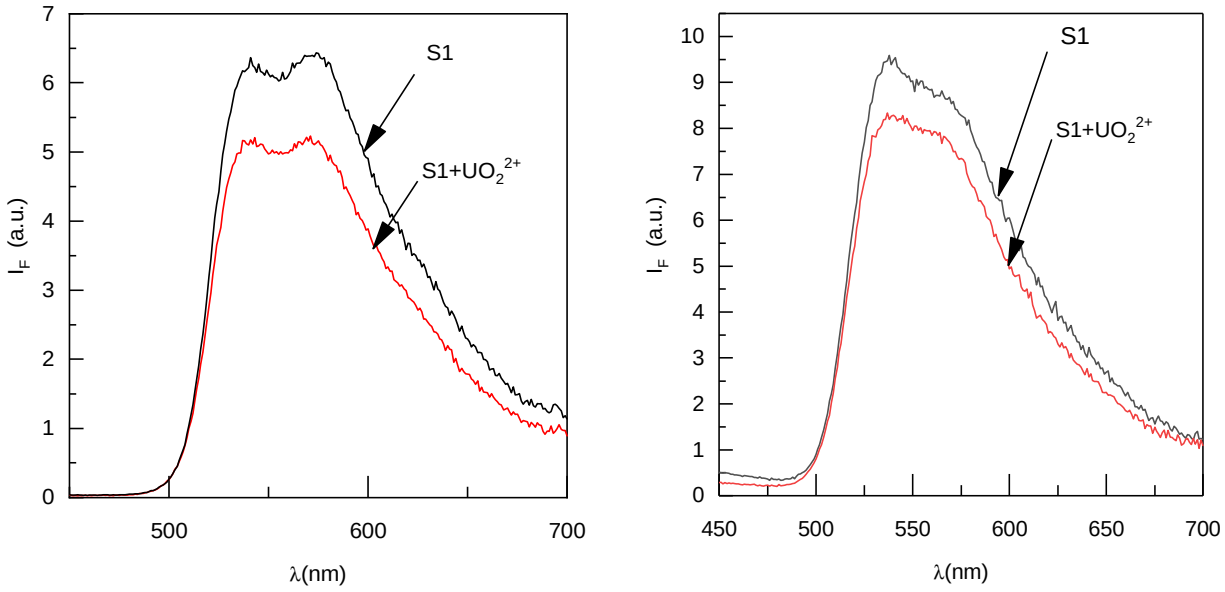

Figure 3. Response of S1 aggregates in water (left) and in water/acetonitrile 9:1 (right) with UO_2^{2+} (50 µM). [S1] = 5 µM, λ_{exc} = 365 nm.

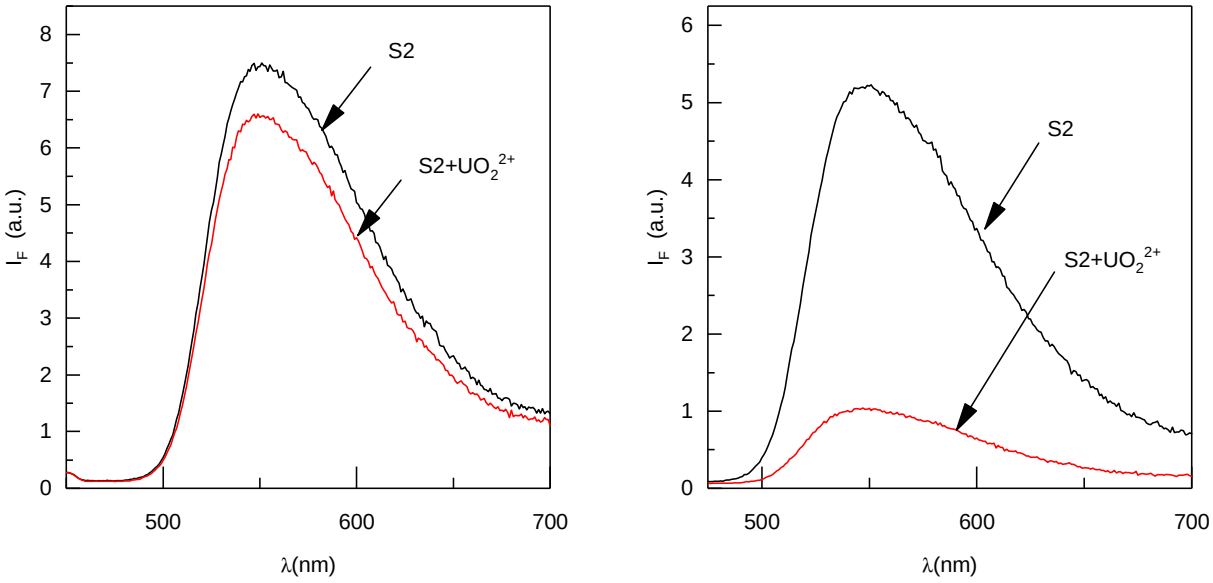

Figure 4. Response of S2 aggregates in water/acetonitrile 8:2 (left) and 6:4 (right) with UO_2^{2+} (50 µM). [S2] = 7 µM, λ_{exc} = 365 nm.

The addition of UO_2^{2+} to S1 aggregates results in slight quenching of fluorescence as shown in Figure 3. Similarly, a small fluorescence decrease was also observed for S2 aggregates at 80% water fraction. However, uranyl complexation with S2 aggregates at 60% water in acetonitrile caused significant

fluorescence quenching (Figure 4). It should be noted that S2 possesses two electron withdrawing $–NO_2$ groups which stabilize phenolate form of S2 in solution and the complexation with uranyl is therefore more efficient. It might be a reason that efficient fluorescence quenching was observed for S2 compared to that for S1. As the response of S2 towards uranyl is more pronounced, we decided to use this ligand for the detailed complexation studies.

Subsequently, complexation kinetics of S2 with uranyl cation (10 µM) was investigated in water/acetonitrile (60/40; v/v). Diffusion in the visible region (Figure 5) which belongs to the aggregates slowly disappeared, implying that the aggregates were gradually destroyed. Interaction of uranyl with the aggregated form of S2 favors the release of individual molecules of S2 as indicated by the gradual increase of absorbance at 365 nm (Figure 5). The measured absorbance at 365 nm reached equilibrium after 30 minutes, suggesting that the minimum time to complete the complexation is about 30 minutes.

The complexation with uranyl was also performed in HEPES buffer/acetonitrile (pH = 7, 60/40; v/v). In comparison to water/acetonitrile system, a similar fluorescence response was noticed in this mixture, showing that the sensor can also work the same way in buffer solution. (Figure S2).

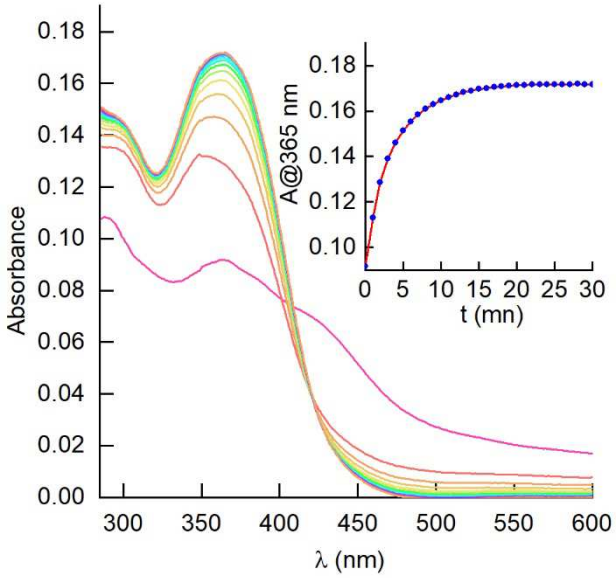

Figure 5. Kinetic of absorbance of S2 (7 µM) in water/acetonitrile (60/40; v/v) upon adding uranyl 10 µM.Inset: absorbance at 365 nm over time.

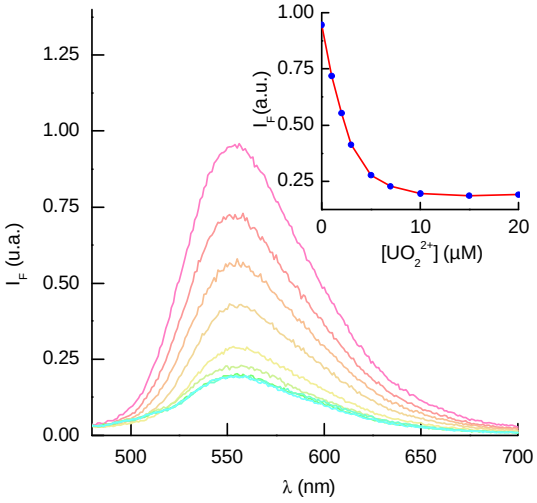

Figure 6. Titration data of S2 (7 µM) with different uranyl concentration. Inset: fluorescence intensities at 550 nm as a function of uranyl concentration in water/acetonitrile (60/40; v/v). λ_{exc} = 365 nm.

Fluorescence titration of S2 with uranyl cation was also performed. Uranyl nitrate was added to aggregates of S2 in water/acetonitrile mixture (60/40; v/v).

Figure 6 shows the changes in fluorescence spectra and intensities at 550 nm as a function of uranyl concentration. The fluorescence titration data was consistent with the aggregate-breaking mechanism as discussed above. The addition of 10 µM of uranyl seemed to destroy the aggregates and considerably quenched the fluorescence. An aggregate-destructive mechanism upon adding uranyl cation was then proposed as shown in Figure 7. Complexation of S2 molecules with uranyl cation actually destroyed the formed aggregates to solubilize the molecules in the solution. Since the required quantity of uranyl for saturated titration was reasonably close to one equivalent, is it possible that the stoichiometry of S2-uranyl complex is 1:1.

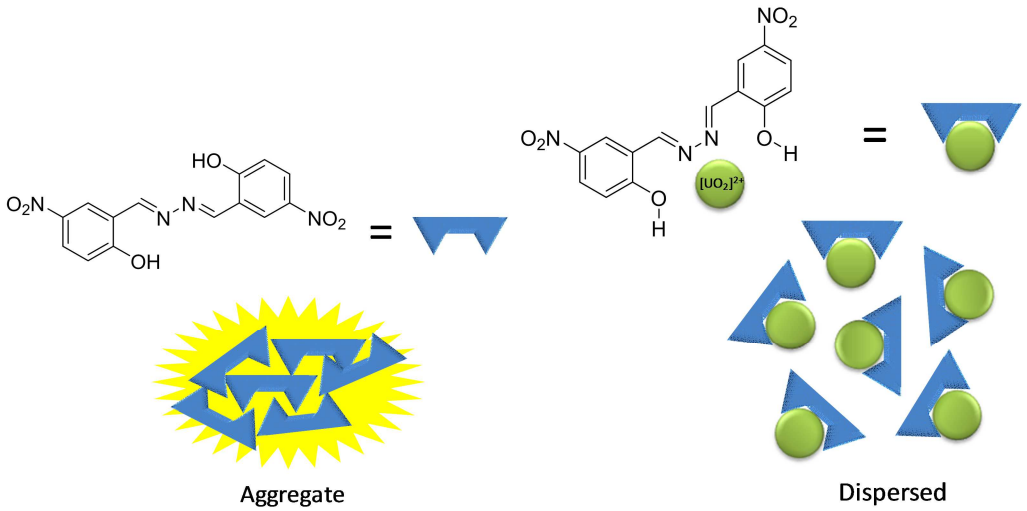

Figure 7. Proposed quenching mechanism of S2 upon uranyl addition.

Study on particle sizes

The destruction of emissive aggregates of S2 upon uranyl complexation was supported by Dynamic Light Scattering (DLS) study. Aggregates of S2 (7 µM) were prepared in water/acetonitrile (60/40; v/v). As shown in Figure 11 (black columns), the average sizes of S2 aggregates are in the range of 350-450 nm. The addition of uranyl (2 µM) to aggregates of S2 partially destroyed them and decreased the average size to about 250-350 nm (Figure 11, red columns). No signal was detected once excess uranyl was added, implying that most of the aggregates were destroyed by uranyl cation. This is consistent with that observed in spectroscopic measurements. In addition, SEM measurements indicated a modification of aggregated forms upon addition of uranyl ions (Fig S3), with SEM images showing the tightly packed aggregates of S2 in water/acetonitrile (60/40; v/v). The addition of uranyl cation (20 µM, one hour) modified the shape of the aggregates, implying that there was a complexation between S2 aggregates and uranyl cations.

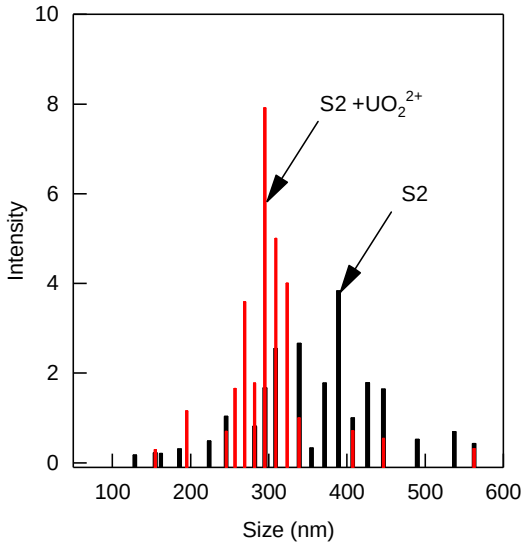

Figure 11. Comparison of DLS data of S2 alone (black columns) and S2 + uranyl mixture (red columns). Reaction time was one hour. Solvent was water/acetonitrile 60:40. [S2] = 7 µM, [uranyl] = 2 µM.

Sensitivity

The detection limit towards uranyl was calculated based on the response of S2 over a small concentration range of uranyl cation (Figure 12). The following equation was used to calculate the detection limit:

$$c_{\text{limit}} = \frac{3s}{k}$$

Where *s* represents the standard deviation of **S2** solution, c_{limit} is the limit of detection and *k* is the slope of the working curve. The limit of detection was found to be 6.2 ppb (23 nM), consistent with the ppb level of some other reported uranyl sensors[15, 16]and exceeding others. [12, 14]

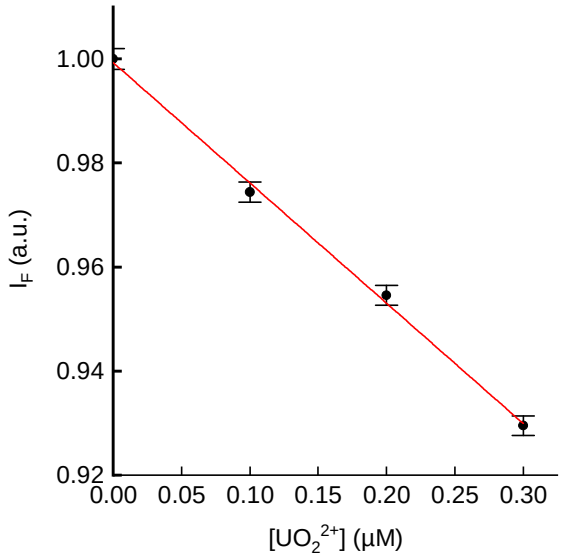

Figure 12. Calibration curve of S2 (7 μM) with small range of [Uranyl] in water/acetonitrile (60/40; v/v). λ_{exc} = 365 nm. Fluorescence intensities were recorded at 550 nm.

Selectivity

In order to evaluate the selectivity of sensor S2 towards uranyl, fluorescence response was measured in the presence of other possible competing cations. It is to be noted that lanthanides have been well known as interfering cations in the nuclear industry analysis. For that reason, three lanthanides (La^{3+}, Ce^{3+} and Yb^{3+}) and other common cations (K^{+}, Ca^{2+}, Mg^{2+}, Cd^{2+}, Zn^{2+}, Hg^{2+}, Fe^{3+}, Al^{3+}) were tested. To avoid the hydrolysis of metal cations, HEPES (pH 7.0) solution was used instead of pure water. In HEPES (pH 7.0)/acetonitrile solution, the absorbance or emission profile of S2 as well as the response with uranyl was very close with that in water/acetonitrile system (Figure S1 and S2). All samples were excited at 365 nm and fluorescence intensities were recorded at 550 nm. As shown in Fig. 13, the effect induced by an addition of 20 μM of competing metal ions were negligible. Upon the addition of 20 μM of uranyl ions, the full response was obtained, indicating that no significant interference results from the presence of these ions. In summary, sensor S2 can efficiently detect uranyl in the presence of a wide range of lanthanides and other common cations for practical application.

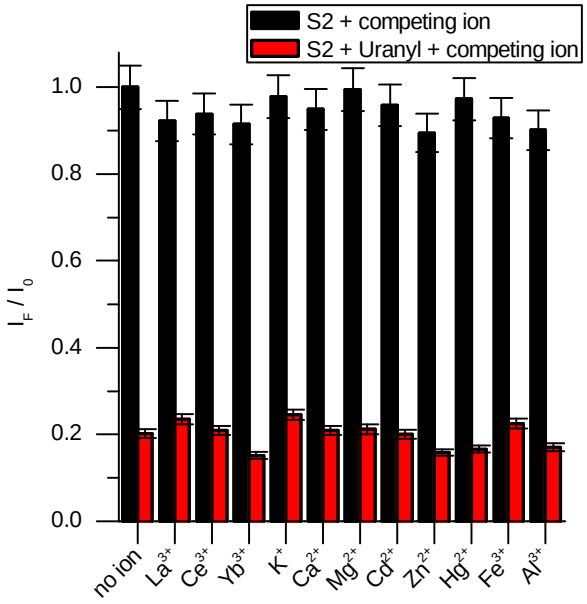

Figure 8. Selectivity of S2 towards uranyl over other metal ions. Reaction time is one hour. Excitation wavelength was 365 nm and all fluorescence values were recorded at 550nm. [S2] = 7 µM, [UO_2^{2+}] = [competing cations] = 20 µM. Uranyl source: uranyl nitrate.

Conclusion

A series of salicylaldehyde azines have been synthesized and studied. In organoaqueous media, compounds S1 and S2 exhibited strong AIE characteristics. Due to oxygen and nitrogen binding sites, the molecules could form complexes with uranyl cations and quench the fluorescence. In the present research, it is to be noted that the effect of uranyl is somewhat more destructive rather than constructive to the aggregation. The strongest quenching effect was observed for the aggregates of S2 in water/acetonitrile (60/40; v/v). The fluorescence quenching is explained by an aggregate-breaking mechanism, as the fluorescent aggregates were destroyed by the complexation with uranyl cation. The proposed mechanism was further supported by DLS and SEM experiments. Sensor S2 shows good selectivity towards uranyl over lanthanides and other common cations, and allows a detection limit of 6.8 ppb for uranyl ions.

Acknowledgements

This work was supported by the National Research Agency program “DECRET” (ANR-13-SECU-0001).

References :

[1] M.G. Bunn, M.B. Malin, N.J. Roth, W.H. Tobey, (2014).

[2] J.L. Domingo, Reproductive Toxicology, 15 (2001) 603-609.

[3] V. Zare-Shahabadi, M. Akhond, J. Tashkhourian, F. Abbasitabar, Sensors and Actuators B: Chemical, 141 (2009) 34-39.

[4] U. Sundar, V. Ramamurthy, V. Buche, D.N. Rao, P. Sivadasan, R. Yadav, Talanta, 73 (2007) 476-482.

[5] R. Piech, B. Baś, W.W. Kubiak, Electroanalysis, 19 (2007) 2342-2350.

[6] H.R. Nassab, A. Souri, A. Javadian, M. Amini, Sensors and Actuators B: Chemical, 215 (2015) 360-367.

[7] M. Grabarczyk, A. Koper, Environ. Monit. Assess., 185 (2013) 5515-5522.

[8] M. Gregusova, B. Docekal, Anal. Chim. Acta, 684 (2011) 142-146.

[9] P.G. Whitkop, Anal. Chem., 54 (1982) 2475-2477.

[10] J.C. Veselsky, B. Kwiecinska, E. Wehrstein, O. Suschny, Analyst, 113 (1988) 451-455.

[11] I. Kochan, I. Shuktomova, J. Radioanal. Nucl. Chem., 188 (1994) 27-32.

[12] S. Maji, K. Viswanathan, J. Lumin., 129 (2009) 1242-1248.

[13] I. DeVore, A. Michael, S.A. Kerns, A.E. Gorden, Eur. J. Inorg. Chem., 2015 (2015) 5708-5714.

[14] C.-T. Yang, J. Han, M. Gu, J. Liu, Y. Li, Z. Huang, H.-Z. Yu, S. Hu, X. Wang, Chem. Commun., 51 (2015) 11769-11772.

[15] A. Elabd, M. Attia, J. Lumin., 169 (2016) 313-318.

[16] J. Ma, W. He, X. Han, D. Hua, Talanta, 168 (2017) 10-15.

[17] X. Chen, L. He, Y. Wang, B. Liu, Y. Tang, Analytica chimica acta, 847 (2014) 55-60.

[18] J. Wen, Z. Huang, S. Hu, S. Li, W. Li, X. Wang, Journal of hazardous materials, 318 (2016) 363-370.

[19] W.-M. Chen, X.-L. Meng, G.-L. Zhuang, Z. Wang, M. Kurmoo, Q.-Q. Zhao, X.-P. Wang, B. Shan, C.-H. Tung, D. Sun, Journal of Materials Chemistry A, 5 (2017) 13079-13085.

[20] J. Ye, R.F. Bogale, Y. Shi, Y. Chen, X. Liu, S. Zhang, Y. Yang, J. Zhao, G. Ning, Chemistry–A European Journal, 23 (2017) 7657-7662.

[21] X. Chen, L. Peng, M. Feng, Y. Xiang, A. Tong, L. He, B. Liu, Y. Tang, Journal of Luminescence, 186 (2017) 301-306.

[22] M. Shamsipur, M. Mohammadi, A.A. Taherpour, A. Garau, V. Lippolis, RSC Advances, 5 (2015) 92061-92070.

[23] M. Ghaedi, J. Tashkhourian, M. Montazerozohori, A.A. Pebdani, S. Khodadoust, Materials Science and Engineering: C, 32 (2012) 1888-1892.

[24] P. Harvey, A. Nonat, C. Platas Iglesias, L. Natrajan, L. Charbonniere, Angewandte Chemie International Edition, (2018).

[25] Y.B. Ruan, A. Depauw, I. Leray, Org Biomol Chem, 12 (2014) 4335-4341.

[26] X.Q. Pham, L. Jonusauskaite, A. Depauw, N. Kumar, J.P. Lefevre, A. Perrier, M.-H. Ha-Thi, I. Leray, Journal of Photochemistry and Photobiology A: Chemistry, 364 (2018) 355-362.

[27] J. Bell, I. Samb, P.Y. Toullec, O. Mongin, M. Blanchard-Desce, V. Michelet, I. Leray, New J. Chem., 38 (2014) 1072-1078.

[28] N. Kumar, Q. Pham-Xuan, A. Depauw, M. Hemadi, N.-T. Ha-Duong, J.-P. Lefevre, M.-H. Ha-Thi, I. Leray, New J. Chem., 41 (2017) 7162-7170.

[29] A. Depauw, N. Kumar, M.H. Ha-Thi, I. Leray, The journal of physical chemistry. A, 119 (2015) 6065-6073.

[30] W.X. Tang, Y. Xiang, A.J. Tong, J. Org. Chem., 74 (2009) 2163-2166.

[31] S. Dalapati, M.A. Alam, S. Jana, S. Karmakar, N. Guchhait, Spectrochimica acta. Part A, Molecular and biomolecular spectroscopy, 102 (2013) 314-318.

[32] A.M. Brouwer, Pure and Applied Chemistry, 83 (2011) 2213-2228.

[33] Y. Gong, Y. Tan, H. Li, Y. Zhang, W. Yuan, Y. Zhang, J. Sun, B.Z. Tang, Science China Chemistry, 56 (2013) 1183-1186.

[34] J.R. Lakowicz, A. Balter, Photochem. Photobiol., 36 (1982) 125-132.

[35] G. Weber, F.J. Farris, Biochemistry, 18 (1979) 3075-3078.

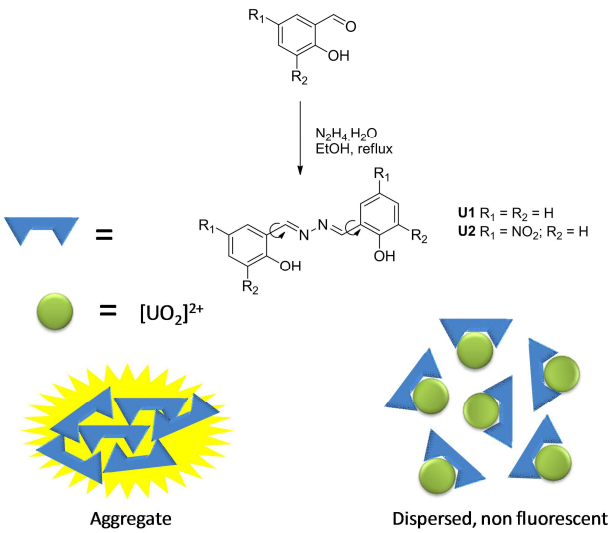
R1
O
OH
R2
N2H4.H2O
EtOH, reflux
U1 R1 = R2 = H
U2 R1 = NO2; R2 = H
=
=
[UO2]2+
Aggregate
Dispersed, non fluorescent

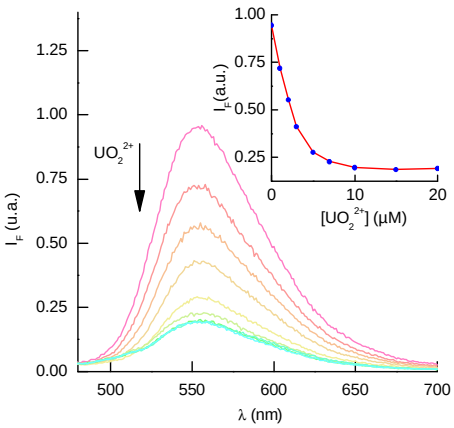
UO2 2+
IF (u.a.)
λ (nm)
IF (a.u.)
[UO2 2+] (μM)